EUROfusion

EUROFUSION WPJET1-PR(14) 12520

Hyun-Tae Kim et al.

Comparative Analysis of Electron Heat Transport of JET High Density H-mode Plasmas with C wall and ITER-Like Wall

Preprint of Paper to be submitted for publication in
Plasma Physics and Controlled Fusion

This work has been carried out within the framework of the EUROfusion Consortium and has received funding from the Euratom research and training programme 2014-2018 under grant agreement No 633053. The views and opinions expressed herein do not necessarily reflect those of the European Commission.

Comparative Analysis of Heat Transport of JET High Density H-mode Plasmas in Carbon Wall and ITER-Like Wall

Hyun-Tae Kim[1], M. Romanelli[1], I. Voitsekhovitch[1], T. Koskela[2], J. Conboy[1], C. Giroud[1], G. Maddison[1], E. Joffrin[3] and JET EFDA contributors*

EUROfusion Consortium, JET, Culham Science Centre, OX14 3DB, Abingdon, UK

[1]CCFE, Culham Science Centre, Abingdon, Oxon, OX14 3DB, UK
[2]Aalto University, Association EURATOM-Tekes, P.O.Box 14100, FIN-00076 Aalto, Finland
[3]CEA, IRFM, F-13108 Saint-Paul-lez-Durance, France
** See annex of F. Romanelli et al, "Overview of JET Results", (25th IAEA Fusion Energy Conference, Saint Petersburg, Russia (2014)).*

Preprint of Paper to be submitted for publication in
Plasma Physics and Controlled Fusion

ABSTRACT

A consistent deterioration of global confinement in H-mode experiments has been observed in JET [1] following the replacement of all carbon Plasma Facing Components (PFCs) with an all metal ('ITER-like') wall (ILW). This has been correlated to the observed degradation of the pedestal confinement, as lower electron temperature (T_e) values are routinely measured at the top of the edge barrier region. A comparative investigation of core heat transport in JET-ILW and JET-CW (Carbon Wall) discharges has been performed, to assess whether core confinement has also been affected by the wall change.

The results presented here have been obtained by analysing a set of discharges consisting of high density JET-ILW H-mode plasmas and comparing them against their counterpart discharges in JET-CW having similar global operational parameters. The set contains 10 baseline ($\beta_N = 1.5\sim2$) discharge-pairs with 2.7T toroidal magnetic field, 2.5MA plasma current, and 14 to 17MW of Neutral Beam Injection (NBI) heating.

Based on a T_e profile analysis using High Resolution Thomson Scattering (HRTS) data, the T_e profile peaking P_e (= core T_e ($\rho = 0.3$) / edge T_e ($\rho = 0.7$)) is found to be similar, and weakly dependent on edge T_e, for JET-ILW and JET-CW discharges. When ILW discharges are seeded with N_2, core and edge T_e both increase to maintain a similar peaking factor.

The change in core confinement properties is addressed with interpretative TRANSP simulations. Although electron heat conductivity χ_e and heat flux q_e are found to be higher, and χ_i and q_i lower, in JET-ILW, this is consistent with the higher NBI power deposition to electrons and the lower NBI power deposition to ions, in ILW discharges where T_e is lower. The TRANSP analysis indicates that the overall core confinement is not degraded in the ILW discharges compared to C-wall.

1. INTRODUCTION

Carbon Plasma Facing Components (PFCs) have been recently replaced in JET with an all metal Beryllium first wall and Tungsten divertor, which comprise the ILW (ITER-Like Wall) [2]. It is well known that the interaction between plasma and the surrounding wall can influence plasma energy confinement significantly as a result of the sputtering of different impurities and modified wall recycling [1]. In addition, the operational techniques required for the ILW (e.g. higher gas fuelling, to avoid W accumulation in the core) differ from those required for CW (Carbon Wall) operation. After the wall change, the global energy confinement was routinely found to be degraded, when compared to similar plasmas in the CW configuration. Core temperatures are found to be lower as are the temperatures at the top of the pedestal [3]. One current research topics at JET is the investigation of the cause for this deterioration [1] [3]. It is well known that the core temperature depends on the temperature at the plasma edge. Since the edge temperature is lower in the ILW configuration, it is not obvious whether the decrease in core temperature is only due to the degradation of the edge confinement or if the core confinement itself has also been degraded.

A transport analysis of 10 pairs of counterpart discharges (10 CW discharges and 10 corresponding

ILW discharges), has been carried out to address this question. Counterpart discharges have been carefully selected to match the average value of the controllable global plasma parameters:–

- 2.5MA of total plasma current I_p,
- 2.7T of toroidal magnetic field B_t,
- 14–17MW of applied NBI power $P_{NBI,}$
- 7.1–10.2×$10^{19}$$m^{-3}$ average electron density $\overline{n}_e$
- safety factor q_{95},
- triangularity δ

- as closely as possible within a reference time window, from t_{ref} – 0.5 s to t_{ref} +0.5s. The reference time t_{ref} is selected during the stationary flat-top phase of the discharge (see Figure 1). This procedure is designed to remove the influence of the global plasma parameters, and allow an investigation of the effects of the different walls on transport processes. It is observed that Z_{eff} in CW shots is much higher than Z_{eff} in the ILW counterparts i.e. Z_{eff} = 1.7~2.4 for CW and Z_{eff} = 1.1~1.3 for ILW. This indicates that the plasma compositions in CW and ILW are different. For CW discharges, Z_{eff} is subject to significant variation even without any impurity seeding. This can be attributed not only to the wall material, but also to the impurity retention from the previous impurity-seeded discharges. On the other hand, the Z_{eff} variation in the ILW discharges is much less significant allowing a higher degree of reproducibility, although small variation can still exist when the discharges are following after impurity-seeded discharges on the same day. It should be noted that the highest Z_{eff} in unseeded ILW discharges is still smaller than the lowest Z_{eff} in CW, but with N_2 seeding in ILW discharges the Z_{eff} increases up to a comparable value in CW.

The analysis reported in this paper is focused on low beta baseline H-mode plasmas. Figure 1 shows a typical example of the counterpart discharges selected *amongst low beta baseline (β_N = 1.5~2) H-mode plasmas, which have high plasma density ($7\times10^{19}\ m^{-3} < \overline{n}_e \leq n_{GW} \approx 9\times10^{19}\ m^{-3}$).* At these level of collisionality, the electron and ion temperature profiles tend to be very similar because of the high equilibration power i.e. $T_e \approx T_i$ ($\approx$ T). High beta hybrid $\beta_N \approx 3$) plasmas [4] have been analysed in Challis et al [5], where it is reported that the power degradation of thermal energy confinement with heating power is weaker in the ILW. The main parameters of the discharges analysed are given in Table 1. In order to minimise the effect of measurement errors, time averaged values are used in this study.

In section 2 we report the comparison of the High Resolution Thomson Scattering T_e profiles between JET-ILW and JET-CW discharges. In section 3, the interpretive analysis of core confinement, using the TRANSP transport analysis code [6] [7] is presented. Further discussion and conclusions are given in sections 4 and 5.

2. ELECTRON TEMPERATURE PROFILE ANALYSIS

Electron temperature (T_e) profiles measured by the High Resolution Thomson Scattering (HRTS)

system are used in the present study [8]. Figure 2 shows that the T_e profiles are fitted using a constrained optimisation method based on tomographic techniques (this method optimises the smoothness function while the calculated profile is constrained by measurements [9]), and then remapped to the flux coordinate computed by EFIT [10]. Figure 3 shows T_e profiles at each reference time t_{ref} (at which each pair of counterpart shots have similar global parameters). The profiles have a constant local temperature gradient in the radial region between $\rho = 0.3 \sim 0.7$, which enables them to be compared using the temperature ratio between the two fixed end points. ρ is the square root of normalized toroidal flux, $\sqrt{\Phi_N}$. In this paper, the temperature ratio (i.e. T_e peaking) is defined as $P_{Te} \equiv T_e(\rho = 0.3)/T_e(\rho = 0.7)$.

Figure 4 shows the variation of core temperature with edge temperature. The error bars σ_i are calculated taking account statistical and systematic errors of the HRTS measurement, i.e. $\sigma^2_i = \sigma^2_{SEM} + \sigma^2_{SYS} = \sigma^2_{sta} / N + (0.05 \times T_e^{core})$. σ_{SEM} is the standard error on the mean of 10 measured values in the reference window. The systematic error σ_{SYS} is calculated as $\sigma^2_{SYS} = (0.05 \times T_e^{core})$, assuming a 5% uncertainty in HRTS T_e measurement comparisons between the ILW and C walls.

The dashed lines in Figure 4 indicate the change from each CW to its counterpart ILW discharge. As discussed in the introduction, the core T_e is found to be lower in ILW, and this is accompanied by the decrease in edge T_e. An important point to note is that both ILW and CW data are well represented by the same linear fit, showing that the core peaking P_{Te} is not significantly modified by the change of PFCs.

Recently it has been observed that nitrogen seeding can help to recover the edge T_e, and the core T_e in turn, although the full recovery of edge T_e to the previous value has not yet been achieved [11]. The seeding of N_2 in ILW discharges (blue filled symbols) has the effect of moving the profiles towards the CW counterparts, along the same trend line – suggesting that the decrease in core T_e for the ILW discharges is due only to the decrease in edge T_e, and not to any degradation in P_{Te}.

3. TRANSPORT ANALYSIS

3.1 INPUT AND ASSUMPTIONS FOR TRANSP ANALYSIS

Core transport has been analysed by using the TRANSP code [6] [7]. For these simulations, electron density and temperature profiles are taken from HRTS (High Resolution Thomson Scattering) measurements. The ion temperature was not directly measured and is assumed to be equal to the electron temperature ($T_i = T_e$), based on the high densities of the selected discharges ($\overline{n}_e > 7 \times 10^{19} m^{-3}$). The dominant impurity is determined by the PFC material i.e. Carbon for JET-CW, and Beryllium for JET-ILW. The impurity density profile is calculated to be proportional to the electron density assuming a uniform Z_{eff} over the whole radius, where Z_{eff} is determined from visible Bremsstrahlung [12]. The bulk radiation input is given by Bolometry measurement [13]; NBI and RF heating are calculated by NUBEAM [6] and TORIC [14], respectively. The q profile is taken from the equilibrium reconstructed by EFIT [10], constrained by the magnetic probe measurements.

3.2 COMPARISON OF TRANSPORT PROPERTIES

Electron and ion heat fluxes q_e, q_i, and heat conductivities χ_e, χ_i are key transport properties to quantify core confinement. However, these transport properties are not measurable directly from experiments. In this paper, the transport properties are calculated by interpretative TRANSP simulations, using the measured input data – {T_e, n_e, P_{rad}, Z_{eff}, I_p, V_{loop}, B_t, applied P_{NBI}, applied P_{RF}, Gas puffing rate, Last Closed Flux Surface (LCFS) } [15]. It should be noted that heat fluxes and conductivities are calculated by solving the energy balance equation. The energy balance equation of electrons is [16]

$$\frac{3}{2}\frac{\partial(n_e T_e)}{\partial t} + \nabla\cdot\Big(\underbrace{\vec{q}_e}_{\text{conductive heat flux}} + \underbrace{\frac{5}{2}\vec{\Gamma}_e T_e}_{\text{convective heat flux}}\Big) = P_e^{\text{source}} \qquad (1)$$

where the electron conductive heat flux is defined as $\vec{q}_e \equiv -\chi_e n_e \nabla T_e$, and ohmic heating, auxiliary heating such as NBI and RF, equilibration power loss, and atomic reaction related power losses are included in the source term ($P_e^{source} = P_{oh}^e + P_{oh}^e + P_{oh}^e - P_{equi}^e - P_{iz}^e - P_{rad}^e - P_{rec}^e$). $n_e(\rho, t)$ and $T_e(\rho, t)$ are given by measured input profiles, and the source terms are either functions of $n_e(\rho, t)$ and $T_e(\rho, t)$ or directly given by measurements e.g. P_{rad}. The particle flux $\vec{\Gamma}_e$ appearing in the convective heat flux is calculated by solving the continuity equation, the balance between the particle sources and losses computed in TRANSP using the measured data. Rearranging equation (1) and integrating over the volume enclosed by the flux coordinate ρ allows one to obtain the radial electron heat flux $\vec{q}_e \cdot \hat{r}_e$ and in turn χ_e ($= -(\vec{q}_e \cdot \hat{r}_e)/(n_e \nabla T_e \cdot \hat{r}_e)$, which is consistent with the input profiles of T_e and n_e.

Figures 5(a) and (b) show the TRANSP calculated conductivities χ_e and χ_i at $\rho = 0.5$. As indicated by the dashed lines, there is a consistent change of conductivities from CW to ILW i.e. an increase in χ_e and decrease in χ_i. Figures 5(c) and (d) show that the total radial heat fluxes for electrons (q_e) and ions (q_i) at $\rho = 0.5$ have similar trends. Although $n_e \nabla T_e$ is higher in CW data ($\langle n_e \rangle$ is one of the matching criterias, but ∇T_e is higher in CW), this does not significantly affect the variation of χ_e and χ_i between CW and ILW.

The observed trend of q_e and q_i can be correlated to the change in NBI power deposition. TRANSP calculates the deposited power with NUBEAM, a NBI module using a Monte Carlo method, which takes into account effects such as shine-though power, Charge Exchange losses, and orbital drift losses [6]. Figure 5(e) and (f) show the TRANSP calculated NBI power deposition to electrons and ions, integrated over the volume $\rho < 0.5$. The NBI heating power to the ions P_{NBI}^i not only shows the qualitative trend of change seen for q_i but also the same magnitude, indicating that P_{NBI}^i is in balance with q_i. The electron heating power P_{NBI}^e also has a variation similar to q_e, but the magnitude of q_e is slightly smaller compared to P_{NBI}^e in CW. This can be attributed to other power sink terms such as radiation P_{rad} and convective power loss terms P_{conv}. Figure 6 shows that the contribution of P_{rad} and P_{conv} are higher for CW in most pairs, and therefore relatively less power is transported by q_e in CW as compared to ILW.

Although $T_i = T_e$ is assumed for the TRANSP simulations in Figure 5, there is a possibility that the core T_i is slightly higher than T_e due to the higher ion heating of NBI. The green filled triangles in Figure 5 indicate the TRANSP results assuming slightly higher T_i profile i.e. $T_i = 1.05T_e$. Due to the high equilibration power in the analysed plasmas, the heat flux and conductivities can be changed even with a small discrepancy in T_i and T_e. However, the amount of variation is comparable between the counterparts since $<n_e>$ is one of the selection criteria i.e. similar equilibration power. In addition, NBI heat deposition is not sensitive to the change of T_i. Therefore, the common trend of change in transport properties in Figure 5 would be still valid, even considering an uncertainty of T_i profiles.

The difference in NBI power deposition between CW and the counterpart ILW discharges can be clearly seen in Figure 6, for one pair of discharges from the database. The total deposited $P_{NBI} (= P^e_{NBI} + P^i_{NBI})$ in ILW is shifted towards the edge ($\rho \sim 0.8$). Since the same total NBI power is applied to the counterparts, this implies that in ILW discharges slightly less NBI power is deposited into the core. This can be seen in Figure 8(a) showing that the total deposited P_{NBI} within the volume $\rho<0.5$ in ILW is smaller than JET-CW.

Within the total deposited NBI power $P_{NBI} (= P^e_{NBI} + P^i_{NBI})$, the fraction of electron and ion heating is a function of local ε_b/T_e, with higher ε_b/T_e resulting in lower ion and higher electron heating fractions [17]. The average value of ε_b/T_e within the volume $\rho<0.5$ is shown in Figure 8(b). ILW discharges have higher ε_b/T_e than their counterpart CW discharges due to the lower core T_e. Therefore the fraction of total NBI power deposition to electrons is larger for ILW as compared to CW. Hence, as can be seen in Figure 4(f) and 7, the heating efficiency of electrons (P^e_{NBI}) within the volume $\rho<0.5$ is larger in ILW plasmas despite the reduction of total NBI power deposition. On the other hand, both the fraction of core ion heating and the total NBI deposition are higher for JET-CW, which results in much greater core P^i_{NBI}. In summary, the analysis above shows that for the same total NBI power, core electron heating is more efficient in ILW plasmas while ion heating is reduced.

It should be noted that the lower fraction of core ion heating in ILW plasmas is attributed to the lower edge T_e, which suggests that by recovering the edge electron temperature, the differences in profile of NBI power deposition between ILW and CW might be removed. As shown by that q_i and q_e are balanced with P^i_{NBI} and P^e_{NBI}, respectively (See Figure5(e)(f) and Figure9(g)(h)), NBI heating is dominant in the core. The energy confinement time calculation is also affected by the NBI power deposition profile.

During the steady state, the electrons (τ^{e}_{core}), ions (τ^{i}_{core}), and plasma (τ^{e+i}_{core}) energy confinement time in the volume within ρ<0.5 are calculated as

$$\tau^{e}_{core}(\rho < 0.5) = \frac{\frac{3}{2}k\int_0^{V'(\rho=0.5)} W^{e}_{th}(\rho)\, dV}{\int_0^{V'(\rho=0.5)} P^{e}_{Total}(\rho)\, dV}$$

where $W^{e}_{th}(\rho) = n_e(\rho)T_e(\rho) - n_e(\rho = 0.5)T_e(\rho = 0.5)$,

$$\tau^{i}_{core}(\rho < 0.5) = \frac{\frac{3}{2}k\int_0^{V'(\rho=0.5)} W^{i}_{th}(\rho)\, dV}{\int_0^{V'(\rho=0.5)} P^{i}_{Total}(\rho)\, dV} \qquad (2)$$

where $W^{i}_{th}(\rho) = n_i(\rho)T_i(\rho) - n_i(\rho = 0.5)T_i(\rho = 0.5)$,

$$\tau^{e+i}_{core}(\rho < 0.5) \quad \frac{\frac{3}{2}k\int_0^{V'(\rho=0.5)} W^{e+i}_{th}(\rho)\, dV}{\int_0^{V'(\rho=0.5)} P^{e+i}_{total}(\rho)\, dV}$$

where $W^{e+i}_{th}(\rho) = W^{e}_{th}(\rho) + W^{i}_{th}(\rho)$, and $P^{e+i}_{total}(\rho) = P^{e}_{total}(\rho) + P^{i}_{total}(\rho)$.

W^{e}_{th} and W^{i}_{th} are the W_{th} stored thermal energy in electrons and ions, and P^{e}_{total} and P^{i}_{total} are the total heating power to electrons and ions, respectively. Figure 9 shows that W^{e}_{th} and W^{i}_{th} in ILW are clearly decreased compared to the counterparts in CW, as observed by the lower core T_e in ILW. However, τ^{i}_{core} in ILW is not reduced compared to the counterpart CW since P^{i}_{total} is also lower in ILW. In other words, this implies that the smaller W^{i}_{th} in ILW is just due to the smaller ion heating in the core, rather than degradation of the core ion confinement. P^{e}_{total} is slightly higher in ILW, and this leads to smaller τ^{e}_{core} in ILW. As a result, the plasma energy confinement time τ^{e+i}_{core} is comparable or slightly smaller in ILW.

DISCUSSION

Figure 10 shows the dimensionless parameter $R|\nabla T_e|/T_e$ at ρ = 0.5, where the major radius R is 3m. An interesting point to note is that $R|\nabla T_e|/T_e$ increases as edge T_e decreases resulting in slightly higher $R|\nabla T_e|/T_e$ in ILW compared to that in CW.

Based on the similar magnitude in q_i with the main heating term P^{i}_{NBI} in Figures 5 (c)(e), q_i is the dominant ion heat loss term in ILW and CW. One candidate to explain anomalous ion heat transport is Ion Temperature Gradient (ITG) modes [18]. An important feature of the ITG turbulence theory is that anomalous ion heat flux rises rapidly above a certain critical value in the normalized temperature gradient $|\nabla T_e|/T_i$ [19]. This sets the maximum gradient of the temperature profile. Any excess auxiliary heating above the critical value would further increase the heat flux while only weakly affecting the core temperature. The predicted threshold for ITG is calculated using the analytical formula derived in reference [20],

$$\frac{R}{L_{Ti}^{ITG}} = \frac{4}{3}(1+\frac{T_i}{T_e})(1+2\frac{\hat{s}}{q}) \text{ for } \frac{R}{L_n} < 2(1+\frac{T_i}{T_e}) \quad (3)$$

where q is safety factor, ŝ is magnetic shear (= $(r/q)(dq/dr)$, and L_n is inverse normalized n_e gradient (= $n_e/\nabla n_e$).(For the discharges in this paper, the condition $T_i \sim T_e$ is assumed based on high n_e.) The required parameters for the calculation are given in Table 1.

Figure 11(a) shows the measured R/L_{Ti} against the ITG threshold values predicted by the empirical formula (3). While in CW the measured R/L_{Ti} are generally close to the ITG threshold values, in the ILW counterparts the measured R/L_{Ti} are higher than the ITG threshold. In addition, the dashed lines indicate that in ILW discharges the increase in measured R/L_{Ti} is much larger than the increase in ITG threshold. Figure 11(b) shows the gyro-bohm normalized ion heat flux q_i^{GB} [21] against measured R/L_{Ti}. As indicated by the dashed line, the increase in q_i^{GB} for ILW discharges are accompanied with the increase in measured R/L_{Ti}, and this suggests that the stiffness factor reduced or the threshold value increased in the ILW counterparts. It is not clear whether this increase in measured R/L_{Ti} (=R/L_{Te}) in ILW is a consequence of the lower edge T_e or of other effects resulting from the presence of the metal wall. Further investigation with Gyrokinetic simulations is needed to explain the observed difference, however such an investigation is outside the scope of this paper.

CONCLUSION

In this paper we have investigated the core transport of high density H-mode discharges to assess whether core confinement has been affected by the change of PFCs. To address the above question, a comparative analysis of the core transport of similar H-mode plasmas with Carbon and ITER-like walls has been presented. The discharges analysed have been carefully selected to have the same main global parameters so that any difference in core transport and confinement can be ascribed to effects linked to the different wall composition.

The analysis carried out with TRANSP shows higher NBI power is deposited towards the plasma edge ($\rho>0.6$), and therefore 1~2MW NBI power is less available in the central region ($\rho<0.5$) of ILW discharges. Lower electron temperature is consistently observed at the top of the pedestal in ILW discharges; as a result, the fraction of NBI deposition to core ions is reduced by lower core T_e while the fraction of power to core electrons is enhanced. The overall result is that for the same total beam power the ILW plasmas analysed have higher core

Similar temperature peaking is observed in both ILW and C-wall plasmas. While the increased power deposited to the electrons in ILW discharges is transported by the increased electron heat conductivity along with radiation and convective losses, the ion heat conductivity is found to be lower in ILW discharges and less power is deposited to the ions. As a result, the core electron energy confinement time is somewhat smaller in ILW discharges, but the core ion energy confinement time is not decreased. The latter result is supported by the observation of an increased inverse temperature gradient scale length in ILW as compared to C-wall discharges, above the ITG linear threshold.

The analysis reported in this paper indicates that the overall core confinement is not degraded in the ILW discharges as compared to C-wall. Since the NBI power deposition depends strongly on the T_e profile and the core transport in ILW discharges, it is likely that high core electron temperatures (comparable to that in CW) and improved plasma performance would be achieved if the edge T_e were recovered.

ACKNOWLEDGMENTS

This work has been carried out within the framework of the EUROfusion Consortium and has received funding from the Euratom research and training programme 2014-2018 under grant agreement number 633053, and from the RCUK Energy Programme [grant number EP/I501045]. The views and opinions expressed herein do not necessarily reflect those of the European Commission. The authors appreciate the scientific coordinators of the CW discharges at JET, S. Brezinsek, T. Loarer, D. McDonald, P. Lang, and G. Sabiene.

REFERENCES

[1]. M. Beurskens, et al, "The effect of a metal wall on confinement in JET and ASDEX Upgrade," Plasma Physics and Controlled Fusion, vol. **55**, no. 12, p. 124043, 2013.

[2]. G. Matthews, et al, "JET ITER-like wall overview and experimental programme," Physica Scripta, vol. 2011, no. **T145**, p. 014001, 2011.

[3]. M. Beurskens, et al, "Global and pedestal confinement in JET with a Be/W metallic wall," Nuclear Fusion, vol. **54**, no. 4, p. 043001, 2014.

[4]. J. Hobirk, et al, "Improved confinement in JET hybrid discharges," Plasma Physics and Controlled Fusion, vol. **54**, no. 9, p. 095001, 2012.

[5]. C. D. Challis, et al, "Improved Confinement in JET High Beta Plasmas with an ITER-Like Wall," Nuclear Fusion, 2014 (submitted).

[6]. R.Goldston, et al, "New techniques for calculating heat and particle source rates due to neutral beam injection in axisymmetric tokamaks," Journal of Computational Physics, vol. **43**, no. 1, pp. 61-78, 1981.

[7]. R. Hawryluk, "An empirical approach to tokamak transport," in Physics of Plasmas close to Thermonuclear Conditions, 1979.

[8]. R. Pasqualotto, et al, "High resolution Thomson scattering for Joint European Torus (JET)," Review of Scientific Instruments, vol. **75**, p. 3891, 2004.

[9]. L. Ingesson, "The Mathematics of some Tomography Algorithms at JET," JET Reports JET-R(99)08, 1999.

[10]. L. Lao, et al, "Reconstruction of current profile parameters and plasma shapes in tokamaks," Nuclear Fusion, vol. **25**, no. 11, p. 1611, 1985.

[11]. C. Giroud, et al, "Impact of nitrogen seeding on confinement and power load control of a high-triangularity JET ELMy H-mode plasma with a metal wall," Nuclear Fusion, vol. **53**, no. 11, p. 113025, 2013.

[12]. H. Meister, et al, "Zeff from spectroscopic bremsstrahlung measurements at ASDEX Upgrade and JET," Review of Scientific Instruments, vol. **75**, no. 10, pp. 4097-4099, Oct 2004.

[13]. K. Mast, et al, "Bolometric diagnostics in JET," Review of Scientific Instruments, vol. **56**, no. 5, pp. 969-971, May 1985.

[14]. R. Budny, et al, "Progress Testing TRANSP-TORIC Simulations of ICRH in JET," in 36th EPS conference on plasma physics, Sofia, Bulgaria, 2009.

[15]. J. Ongena, et al, "Numerical Transport Codes," Transactions of Fusion Science and Technology, vol. **33**, pp. 181-191, 1998.

[16]. S.I. Braginskii, "Transport Processes in a Plasma," Reviews of Plasma Physics, vol. **1**, p. 205, 1965.

[17]. J. Wesson, et al, Tokamaks, CLARENDON PRESS OXFORD, 2004.

[18]. P. Mantica, et al, "A Key to Improved Ion Core Confinement in the JET Tokamak: Ion Stiffness Mitigation due to Combined Plasma Rotation and Low Magnetic Shear," Physical Review Letters, vol. **107**, p. 135004, Sep 2011.

[19]. X. Garbet, et al, "Profile stiffness and global confinement," Plasma Physics and Controlled Fusion, vol. **46**, no. 9, p. 1351, 2004.

[20]. S. Guo, et al, "The linear threshold of the ion temperature gradient driven mode," Physics of Fluids B: Plasma Physics (1989-1993), vol. **5**, no. 2, pp. 520-533, 1993.

[21]. P. Mantica, et al, "Experimental Study of the Ion Critical-Gradient Length and Stiffness Level and the Impact of Rotation in the JET Tokamak," Physical Review Letters, vol. **102**, p. 175002, Apr 2009.

	Pulse No:	t_{ref}	B_t [T]	I_P [MA]	Applied P_{NBI} [MW]	$\langle\varepsilon_b/T_e\rangle$ $\rho<0.5$	Applied P_{ICH} (MW)	$\langle T_e\rangle$ [keV] ($\rho<0.5$)	$\langle n_e\rangle$ [10^{20} m^{-3}] ($\rho<0.5$)	$\langle Z_{eff}\rangle$	upper δ at $\rho=1$	$\hat{S}$ at $\rho=0.5$	q at $\rho=0.5$
CW	79453	20	2.7	2.5	14	13	1	3.6	0.92	2.09	0.45	0.68	1.40
ILW(N2)	82819	15	2.7	2.48	16	15	0	3.0	0.92	1.72	0.40	0.79	1.28
CW	79435	20	2.7	2.5	14	16	0	3.0	1.02	1.69	0.44	0.66	1.40
ILW(N2)	82811	15	2.7	2.48	16.4	17	0	2.6	0.98	1.79	0.39	0.77	1.28
CW	77428	15	2.7	2.5	17	12	0	4.2	0.71	1.58	0.18	0.66	1.54
ILW(N2)	83182	15	2.7	2.48	16	17	0	2.7	0.79	1.50	0.19	0.74	1.35
CW	79747	16	2.7	2.5	15	13	0	3.5	0.72	1.80	0.18	0.69	1.51
ILW	83175	15	2.7	2.5	14.8	18	0	2.4	0.83	1.11	0.19	0.63	1.39
CW	79441	20	2.7	2.5	14	14	1	3.2	0.90	1.65	0.44	0.67	1.39
ILW	82751	15	2.7	2.48	16	19	0	2.2	0.81	1.26	0.38	0.70	1.33
CW	77424	15	2.7	2.5	15	12	0	4.3	0.71	2.38	0.18	0.65	1.55
ILW	83177	15	2.7	2.47	16.7	19	0	2.3	0.82	1.23	0.18	0.65	1.41
CW	74312	20	2.7	2.5	14	15	1	3.8	0.86	1.59	0.43	0.69	1.37
ILW	85406	12	2.7	2.5	16.4	19	0	2.3	0.80	1.04	0.37	0.71	1.32
CW	74313	20	2.7	2.5	15	18	1	2.9	0.89	1.65	0.41	0.63	1.40
ILW	85407	12	2.7	2.5	15.6	20	0	2.2	0.84	1.03	0.37	0.72	1.32
CW	76666	20	2.7	2.5	14.9	14	1.2	3.6	0.91	1.93	0.44	0.71	1.37
ILW*	82549	15	2.7	2.5	15	19	2	2.3	0.86	1.27	0.38	0.69	1.31
CW*	76677	20	2.7	2.5	13.9	14	1.7	3.7	0.96	1.95	0.44	0.69	1.38
ILW*	82558	15	2.6	2.6	14.9	19	1.4	2.4	0.79	1.25	0.38	0.69	1.31

*Table 1: Plasma parameters of counterpart discharges in Carbon Wall and in ITER-Like Wall . (N2) shows N_2 seeded discharges. * indicates (unseeded) discharges after seeded discharges on the same day.*

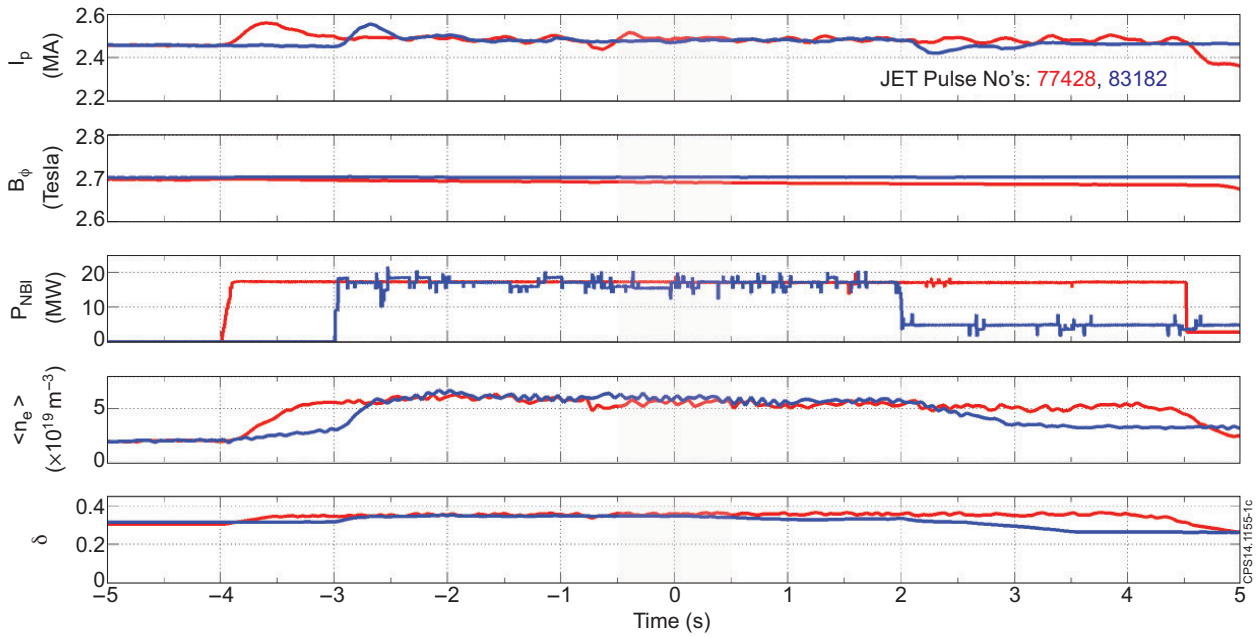

Figure 1:A typical example of counterpart H-mode plasmas in CW (Red) and ILW (Blue). The counterpart discharges having similar controllable global parameters (I_p, B_t, P_{NBI}, $<n_e>$, q_{95}, and δ) around the reference time t_{ref} (indicated with 0).

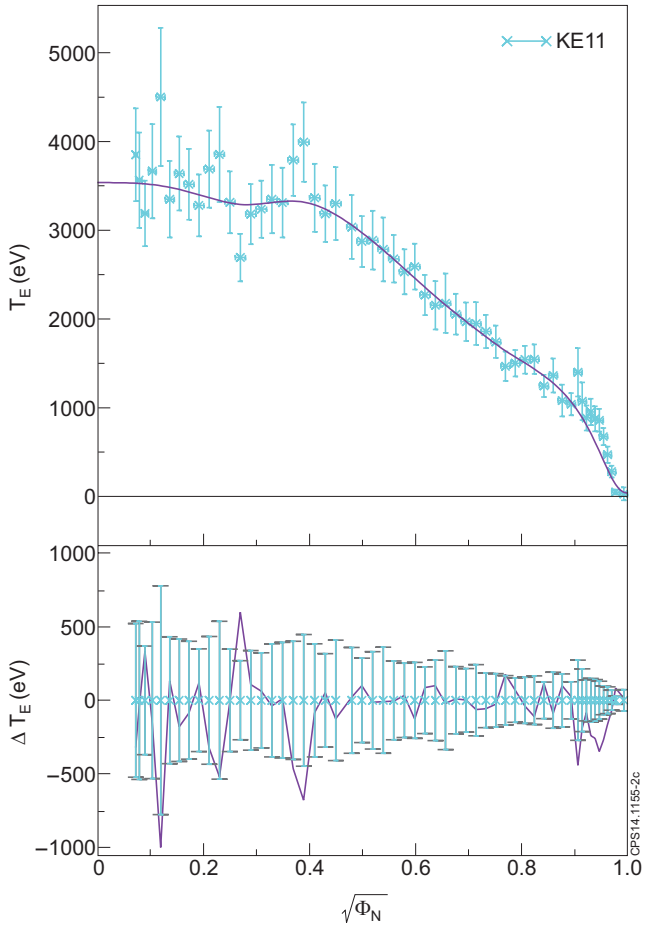

Figure : Remapped HRTS T_e profile (Pulse No: 82819, 15seconds). ΔT_e shows the deviation of the fitting lines from measured data points.

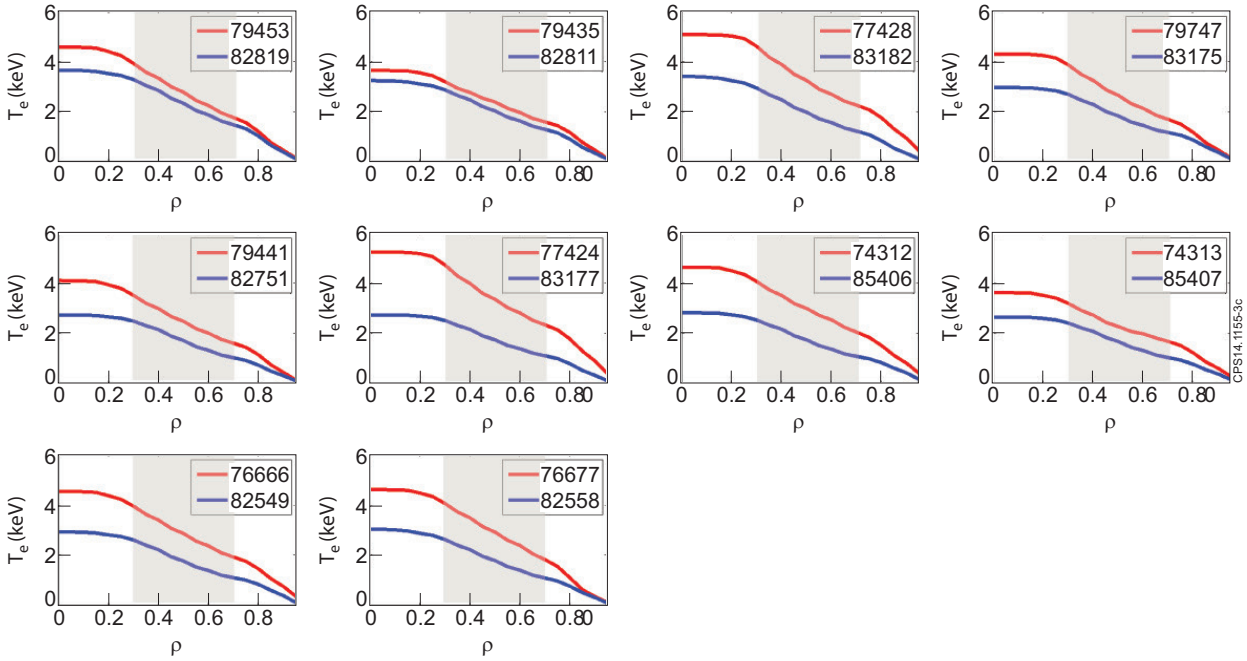

Figure 3: Electron temperature profiles of counterpart discharges in CW (red) and ILW (blue) measured by HRTS (High Resolution Thomson Scattering) and mapped on TRANSP radial coordinate (fitting applied). In the analysed region (i.e. ρ = 0.3~0.7), T_e profiles show a linear increase, justifying the profile analysis based on P_{Te}(i.e. T_e(ρ = 0.3)/T_e(ρ = 0.7)).

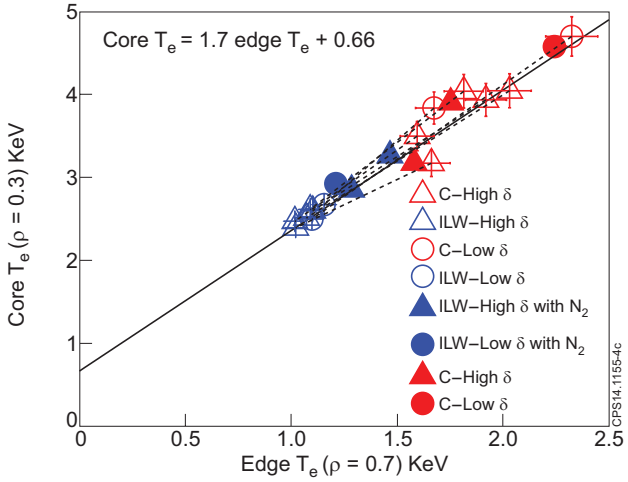

Figure 4: Core T_e(ρ = 0.3) versus Edge T_e(ρ = 0.7). The blue and red symbols indicate ILW and CW plasmas respectively. Dashed lines indicate the change from CW to the counterpart ILW discharge for N_2 seeded plasmas. Blue filled symbols are N_2 seeded ILW plasmas, and red filled symbols are their counterparts in CW. Blank symbols are without impurity seeding. The triangles and circles indicate high and low δ, respectively. The black solid line is a linear fit to the unseeded ILW+CW plasmas, and shows that the N_2 seeded plasmas are positioned between the unseeded ILW and CW discharges.

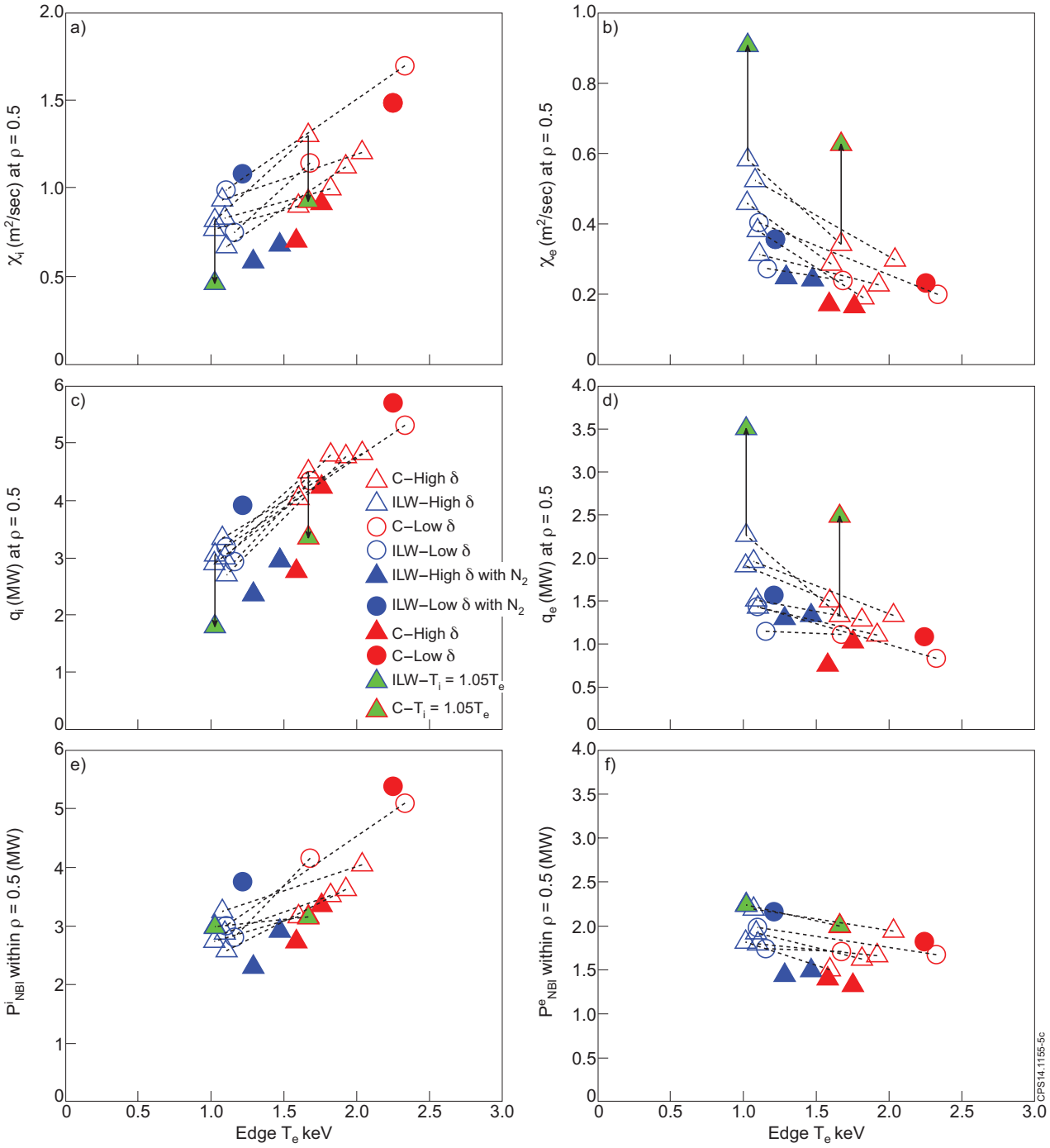

Figure 5: (a)(b) Heat conductivity of ion χ_i and electron χ_e at ρ = 0.5 versus edge T_e (c)(d) Total heat flux of ion q_i and electron q_e at ρ = 0.5 (e)(f) NBI power deposition to ion P^i_{NBI} and electron P^e_{NBI} within the volume **ρ<0.5** *. For all figures x axis is edge T_e at ρ = 0.7. Each dashed line indicates the counterpart data to show the change of the data from JET-CW to JET-ILW. The green filled triangles indicate the TRANSP results with $T_i = 1.05T_e$. Otherwise, the notation of colour and symbols are same as described in Figure 3.*

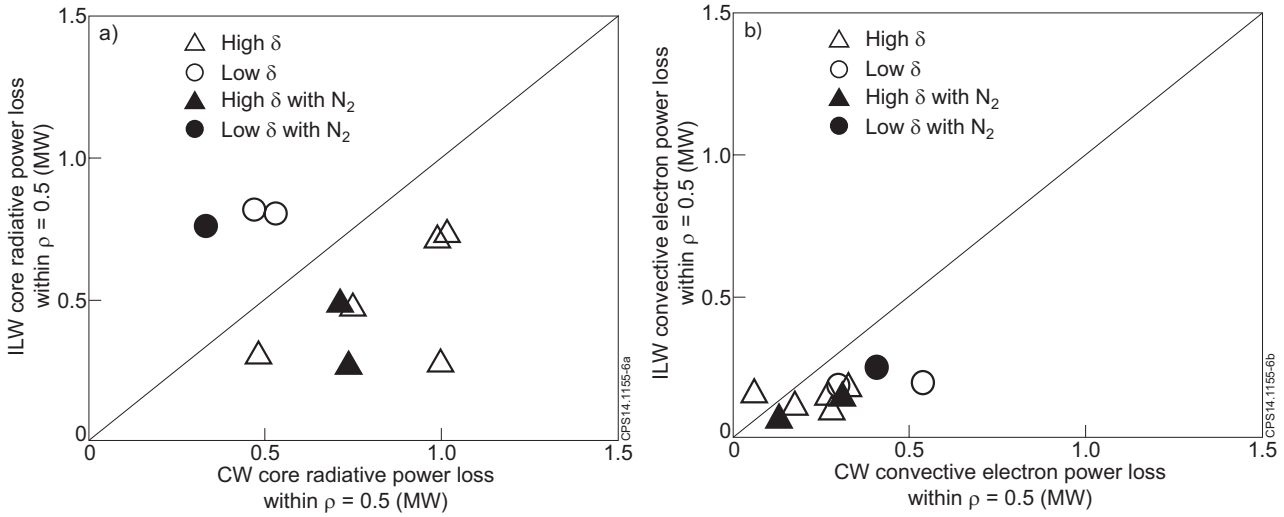

Figure 6: (a) Core radiation comparison within the volume ρ < 0.5 between CW (x axis) and ILW (y axis). (b) Convective electron power loss within the volume ρ < 0.5 between CW (x axis) and ILW (y axis). Triangle and circles are high and low δ, and the filled and blank symbols indicate N_2 seeded and unseeded plasmas, respectively.

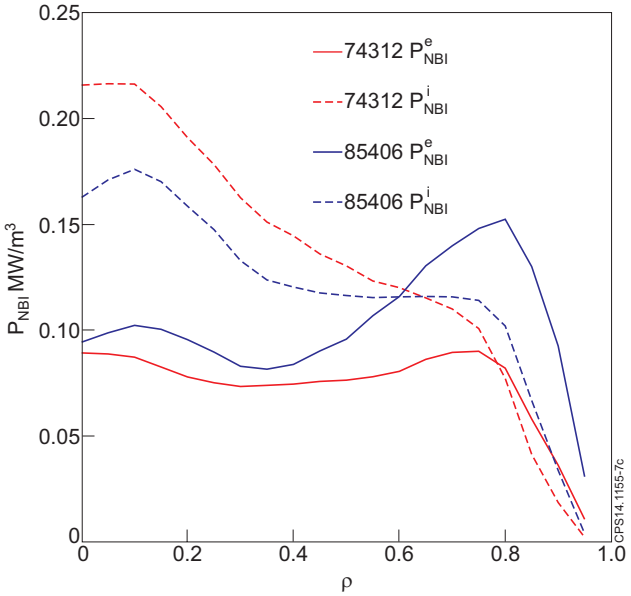

Figure 7: NBI power deposition to electron (solid) and ion (dotted) in JET-ILW (blue) and the counterpart JET-CW(red).

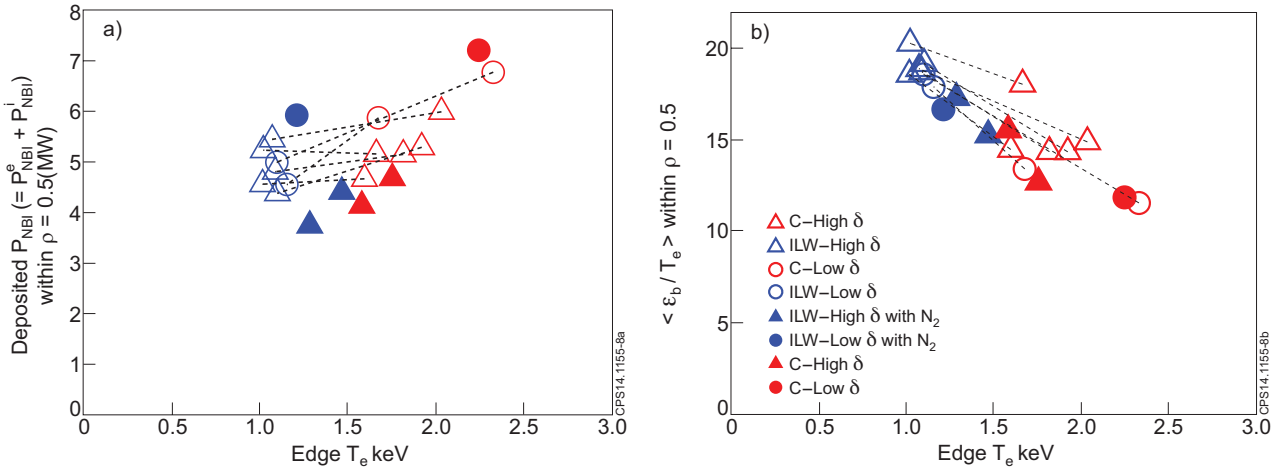

Figure 8: (a) Total deposited beam power P_{NBI} (= P^e_{NBI} + P^i_{NBI}) within the volume ρ < 0.5 (b) averaged value of ε_b/T_e over the volume ρ < 0.5. Each dashed line indicates the counterpart data to show the change of the data from the CW to the ILW. The notation of colour and symbols are same as described in Figure 3.

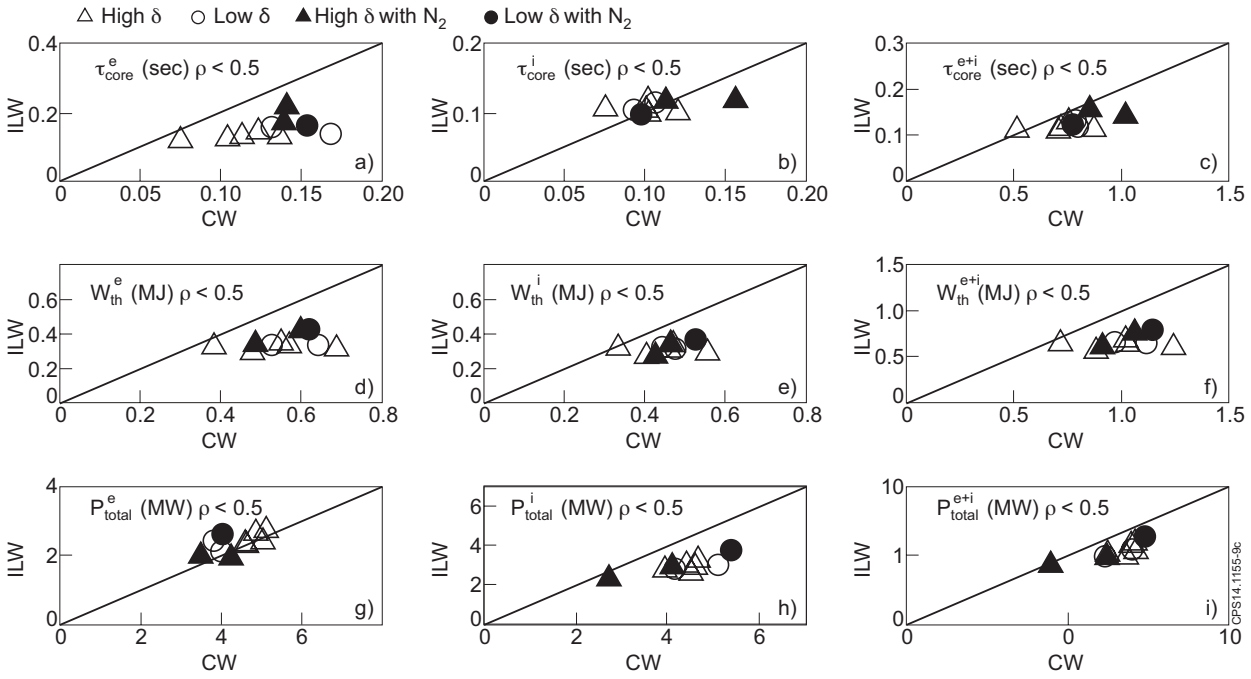

Figure 9: Comparison of energy confinement time in the volume within ρ<0.5: (a)electrons τ^e_{core}, (b) ions τ^i_{core}, (c) plasma τ^{e+i}_{core} between ILW and the counterpart in CW. Comparison of the stored thermal energy in the volume within ρ<0.5: (d)electrons W^e_{th}, (e) ions W^i_{th}, (f) plasma W^{e+i}_{th}. Comparison of the total heating power in the volume within ρ<0.5: (g)electrons P^e_{total}, (h) ions P^i_{total}, (i)plasma P^{e+i}_{total}.

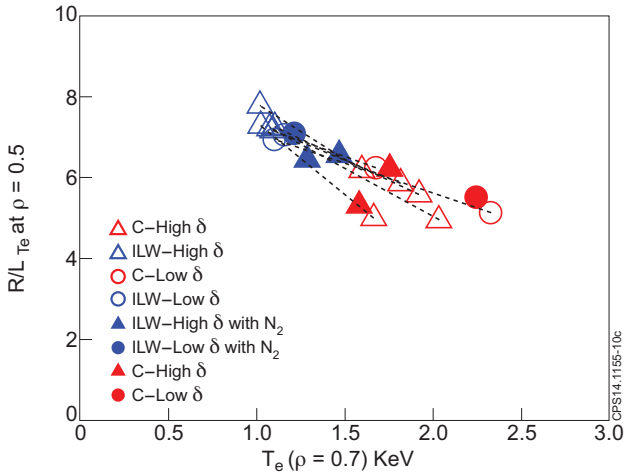

Figure 10: Inverse T_e gradient length R/L_{Te} (at ρ = 0.7) versus edge T_e (= T_e at ρ = 0.7) is larger in ILW plasmas.

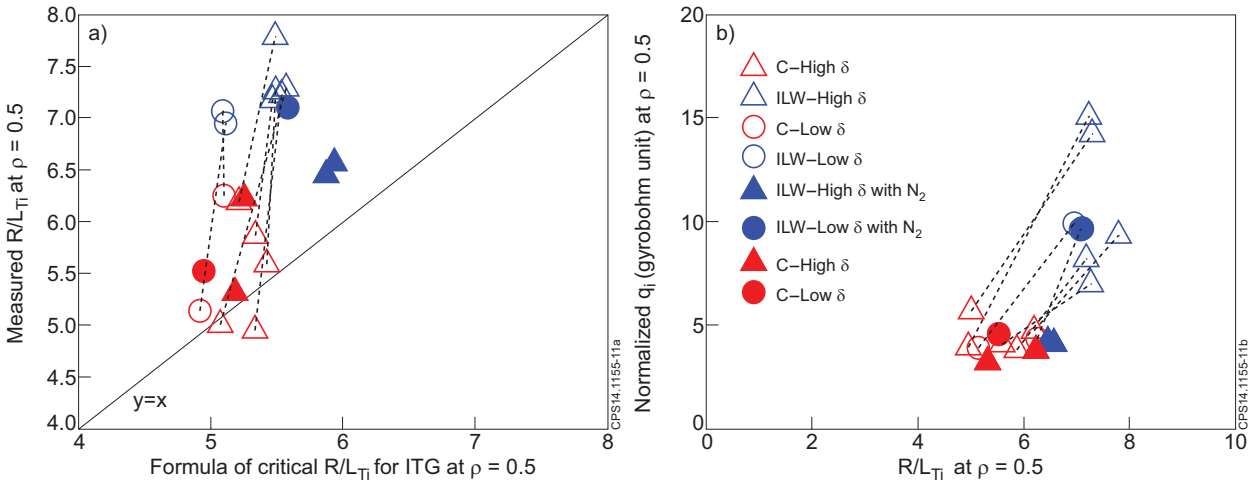

Figure 11: (a)Measured R/L_{Ti} (= R/L_{Te}) versus threshold R/L_{Ti} for ITG mode. (b)gyro-bohm normalized ion heat flux q_i^{GB} [=$q_i/[\rho_i/R)^2\, v_{ith}\, n_i T_i$] with $\rho_i = (T_i m_i)0.5/eB$, $v_{ith} = (T_i/m_i)^{0.5}$ versus measured R/L_{Ti} (=R/L_{Te})